Detection of changes in membrane potential by magnetic resonance imaging

Kyeongseon Min,[1] Sungkwon Chung,[2] Seung-Kyun Lee,[3,4] Jongho Lee,[1] Phan Tan Toi,[3,4] Daehong Kim,[5] Jung Seung Lee,[3,4] and Jang-Yeon Park[3,4,6,*]

[1]Department of Electrical and Computer Engineering, Seoul National University, Seoul, Republic of Korea
[2]Department of Physiology, Sungkyunkwan University School of Medicine, Suwon, Republic of Korea
[3]Department of Biomedical Engineering, Sungkyunkwan University, Suwon, Republic of Korea
[4]Department of Intelligent Precision Healthcare Convergence, Sungkyunkwan University, Suwon, Republic of Korea
[5]National Cancer Center, Goyang, Republic of Korea
[6]Lead contact
[*]Correspondence: jyparu@skku.edu

Summary

Membrane potential plays a crucial role in various cellular functions, particularly in neuronal activation. However, existing techniques for measuring membrane potential are often invasive or have limited recording depth. In contrast, magnetic resonance imaging (MRI) offers noninvasive imaging with desirable spatial resolution across a wide range. This study investigates the feasibility of utilizing MRI to detect membrane potential changes by measuring magnetic resonance parameters while manipulating the membrane potential in cultured cells and a rat model. The findings reveal that depolarization (or hyperpolarization) of the membrane potential leads to increased (or decreased) T_2 relaxation times, while the macromolecular proton fraction shows an inverse relationship.

Keywords

Magnetic resonance imaging; membrane potential; quantitative MRI; craniotomy

Highlights

• Changes in membrane potential can be detected using magnetic resonance imaging (MRI).

• T_2 relaxation time and magnetization transfer are sensitive to changes in membrane potential.

Introduction

Membrane potential is a fundamental property of all living cells, influencing crucial cell functions[1] such as neuronal and myocyte excitability, volume control, cell proliferation, and secretion. In the fields of neuroscience, membrane potential is of significant importance, as neural activities arise from the dynamic propagation of this electric potential. From a clinical perspective, deviations from normal membrane potential levels contribute to various diseases, including seizures[2], arrhythmia[3], and hypoglycemia[4]. Given its scientific and clinical importance, effective methods to detect changes in membrane potential have long been sought.

The intracellular recording technique using sharp glass electrodes is a commonly used method to detect changes in membrane potential[5,6]. It provides real-time absolute recordings of membrane potential. Optical imaging is another major approach to detect changes in membrane potential. Voltage-sensitive dyes enable voltage imaging at the cellular level[7]. Fluorescent calcium indicators detect calcium transients associated with neuronal activation[8]. Label-free optical imaging techniques[9] utilize various contrast mechanisms such as cell membrane deformation, which are directly coupled with changes in membrane potential. Despite their efficacy, these methods have limitations when applied to intact biological systems due to their invasive nature, requiring procedures such as craniotomy.

As noninvasive techniques for directly or indirectly detecting brain activation *in vivo*, several imaging modalities have been developed, including electroencephalography (EEG)[10], magnetoencephalography (MEG)[11], and magnetic resonance imaging (MRI)[12]. EEG and MEG detect electric potentials on the scalp and extracranial magnetic fields, respectively, which are directly induced by neuronal activity in the brain. Although these techniques are noninvasive and provide excellent temporal resolution of milliseconds or less, they are constrained by shallow imaging depth and spatial localization challenges[13].

In contrast, MRI enables noninvasive imaging with good spatial resolution of millimeters over a large brain volume, making it an appropriate tool for functional brain imaging *in vivo*. To date, the mainstream of functional MRI (fMRI) utilizes hemodynamic responses driven by brain activation, such as the blood oxygen level-dependent (BOLD) effect[14]. However, while the BOLD contrast mechanism reflects dynamic changes in neuronal activity through neurovascular coupling, it provides inherently indirect and relatively slow, hemodynamic-responsive information of brain function[15]. On the other hand, many studies have attempted to explore the possibility of using MRI to directly detect neuronal activity[16]. The neuronal current model has primarily been employed for the direct detection of neuronal activity using MRI[17-20], while concerns about sensitivity exist[21-23]. Other than the neuronal current model, direct imaging of neuronal activity (DIANA) was recently proposed and demonstrated promising results in terms of millisecond temporal resolution and neuronal activity correlation[24].

In this study, we investigated the possibility of using MRI to detect changes in membrane potential. Spin-spin relaxation time (T_2) and magnetization transfer (MT) were explored for their dependence on membrane potential changes, both *in vitro* and *in vivo*. *In vitro* experiments utilized two homogeneous and electrically non-active cells, i.e., neuroblastoma (SH-SY5Y) and leukemia (Jurkat) cell lines, providing a controlled environment free from hemodynamic effects. This aided in accurately evaluating changes in MR parameters with membrane potential. *In vivo* experiments, conducted on a rat model with a craniotomy-exposed cortex, aimed to reproduce the *in vitro* findings.

Results

In vitro changes in MR parameters induced by membrane potential

A non-excitable cancerous neuron cell line, SH-SY5Y, was selected to investigate the relationship between MR parameters and membrane potential. Following the culturing of SH-SY5Y cells, they were suspended in extracellular media with various K^+ concentrations ($[K^+]$). As the control condition, $[K^+]$ = 4.2 mM was selected. For depolarization conditions, $[K^+]$ = 20, 40, and 80 mM were used. For hyperpolarization conditions, $[K^+]$ = 0.2 and 1 mM were used. The suspended cells were concentrated with centrifugation in an acrylic container and were then scanned in the 9.4 T preclinical MRI system (BioSpec, Bruker) to measure T_2 and MT parameters such as the pool size ratio (PSR) and the magnetization transfer

rate (k_{mf}) under each condition (Fig. 1). The PSR value represents the ratio of hydrogen protons in macromolecules and free water, and k_{mf} represents the magnetization transfer rate of hydrogen protons from macromolecules to free water. The membrane potential of SH-SY5Y cells in each condition was separately measured via patch clamp recording.

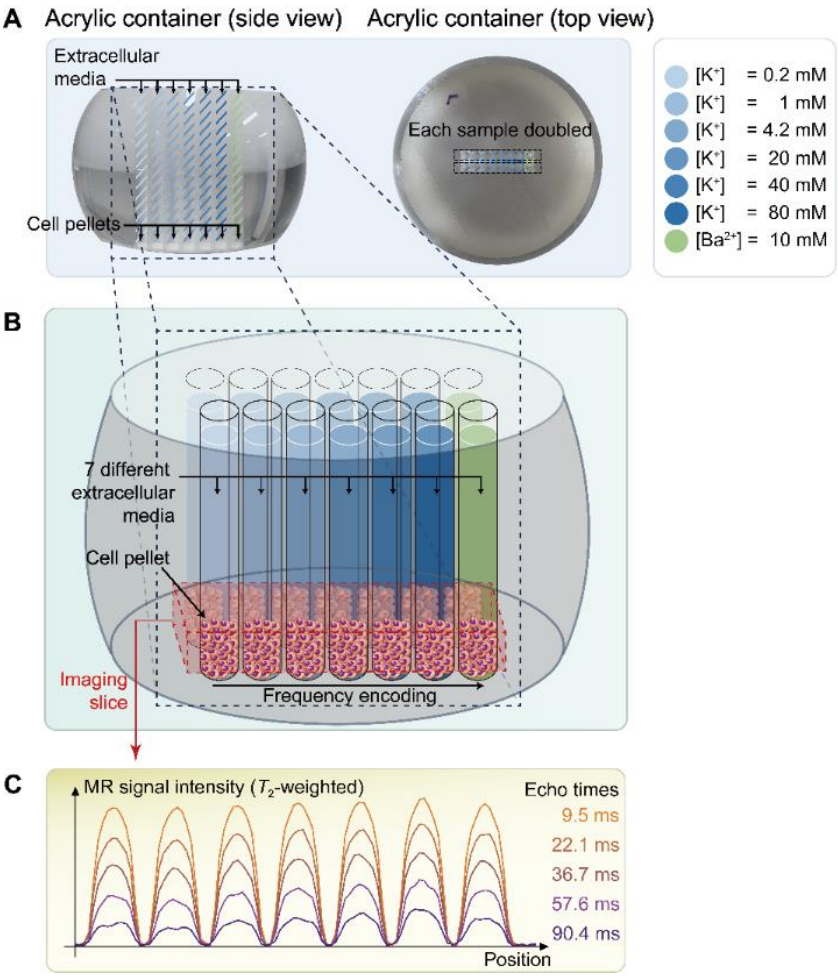

Fig. 1. The schematic diagram of the *in vitro* experiment. (A) The picture on the left displays a side view of a double-sided cut spherical acrylic container with fabricated wells filled with extracellular media and cell pellets. As depicted in the top-view picture on the right, fourteen wells (matrix = 2 × 7) were created on the acrylic container, allowing each of the seven samples with six different K^+ concentrations ($[K^+]$ = 0.2 to 80 mM) and one Ba^{2+} concentration ($[Ba^{2+}]$ = 10 mM) to be doubled in the same column for improved signal-to-noise ratio (SNR) in MR signal acquisition. (B) The image illustrates the configuration after loading cells into the wells and pelleting them at the bottom of the wells. (C) Representative one-dimensional T_2-weighted MR signals with different echo times.

SH-SY5Y cells exhibited significant changes in T_2 and PSR when the membrane potential (V_m) was altered by $[K^+]$ (Fig. 2). The change in T_2 was positive during depolarization, whereas it was negative in PSR. Conversely, during hyperpolarization, the changes in T_2 and PSR were opposite. For example,

during the depolarization (ΔV_m = 30.2 mV) induced by the highest [K^+] = 80 mM, the changes of MR parameters were ΔT_2 = 20.0 ± 2.35% and ΔPSR = −12.8 ± 4.4%, respectively. Conversely, during the hyperpolarization (ΔV_m = −5.3 mV) induced by the lowest [K^+] = 0.2 mM, the changes of MR parameters were ΔT_2 = −4.41 ± 1.96% and ΔPSR = 6.46 ± 6.09%, respectively. However, the change in k_{mf} was not significant in all cases. Statistical significance was tested using one-sample t-test (n = 15), with p-values Bonferroni-corrected for the number of comparisons, which was 6.

Results from *in vitro* SH-SY5Y cell experiments suggest that MR parameters, such as T_2 and PSR, exhibit sufficient sensitivity to detect alterations in membrane potential due to depolarization and hyperpolarization. Furthermore, the changes observed in MR parameters were presented alongside the actual changes in membrane potential measured by patch clamp recordings (Fig. 2). Linear regression analysis between MR parameters and membrane potential showed the following relationship:

$$\Delta T_2\ (\%) = 0.676\ (\%/\text{mV}) \times V_m + 24.3\%\ (p < 0.001)$$

$$\Delta PSR\ (\%) = -0.553\ (\%/\text{mV}) \times V_m - 18.2\%\ (p < 0.001)$$

$$\Delta k_{mf}\ (\%) = 0.0757\ (\%/\text{mV}) \times V_m + 3.22\%\ (p > 0.05)$$

where the p-values of linear coefficients were Bonferroni-corrected for the number of comparisons, which was 3.

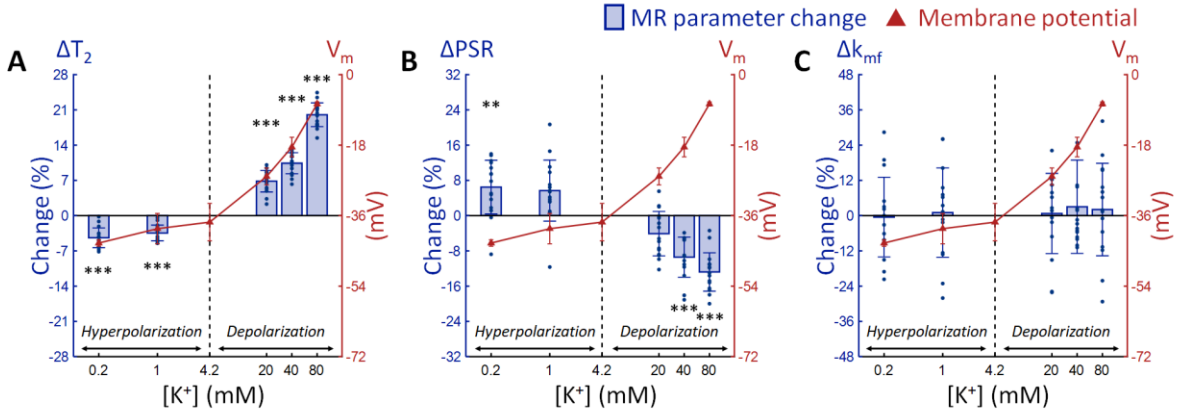

Fig. 2. Changes in MR parameters and membrane potential (V_m) of SH-SY5Y cells versus extracellular K^+ concentrations ([K^+]). Changes in MR parameters such as (A) T_2, (B) PSR, and (C) k_{mf} (blue bar; n = 15) are expressed as percentage changes relative to the control condition of [K^+] = 4.2 mM. Membrane potentials are also plotted alongside changes in MR parameters (red triangle; n = 3). The abscissa is in logarithmic scale. Error bars denote standard deviation. Statistical significance of changes in MR parameters is marked with asterisks (*: p < 0.05, **: p < 0.01, ***: p < 0.001; Bonferroni-corrected).

Using a K^+ channel blocker. For further validation, a depolarization condition was also created by introducing a K^+ channel blocker, [Ba^{2+}] = 10 mM. The resting membrane potential is predominantly governed by K_{2P} channels, and Ba^{2+} is known to block several types of K_{2P} channels[25,26]. For this reason, in this experiment, Ba^{2+} was utilized to decrease the K^+ permeability of the cell membrane, resulting in

depolarization of the resting potential. Ba^{2+}-induced depolarization in SH-SY5Y and Jurkat cells has been reported in previous studies[27,28].

The Ba^{2+}-induced depolarization condition was compared with other depolarization and hyperpolarization conditions induced by varying $[K^+]$ (Fig. 3). The changes in T_2 and PSR in response to depolarization caused by $[Ba^{2+}]$ = 10 mM were measured as ΔT_2 = 7.90 ± 3.72% and ΔPSR = −7.75 ± 6.12%. The actual depolarization of membrane potential induced by $[Ba^{2+}]$ was measured as ΔV_m = 13.3 mV by patch clamp recording. The change in k_{mf} was not significant. Statistical significance was tested using one-sample t-test (n = 15), with p-values Bonferroni-corrected for the number of comparisons, which was 6.

To compare the effect of $[Ba^{2+}]$ on MR parameters with that of $[K^+]$, linear regression analysis was used to assess the significance of the differences in the effects induced by $[Ba^{2+}]$ and $[K^+]$ (Fig. 3). The linear regression analysis revealed that the interaction between the depolarization in membrane potential and the method of depolarization (i.e. $[Ba^{2+}]$ or $[K^+]$) is not significant ($p > 0.05$) for all cases, suggesting that the same degree of depolarization resulted in the same degree of changes in T_2 and PSR, regardless of whether the depolarization was caused by K^+ or Ba^{2+}.

These findings imply that membrane potential-induced changes in T_2 and PSR are not limited to specific methods of altering the membrane potential, such as varying $[K^+]$ or employing Ba^{2+} as a channel blocker. In other words, if the MR parameter changes observed in K^+-experiments were not primarily due to membrane potential changes but rather to other K^+-related factors, MR parameter changes may not have been observed in Ba^{2+}-experiments.

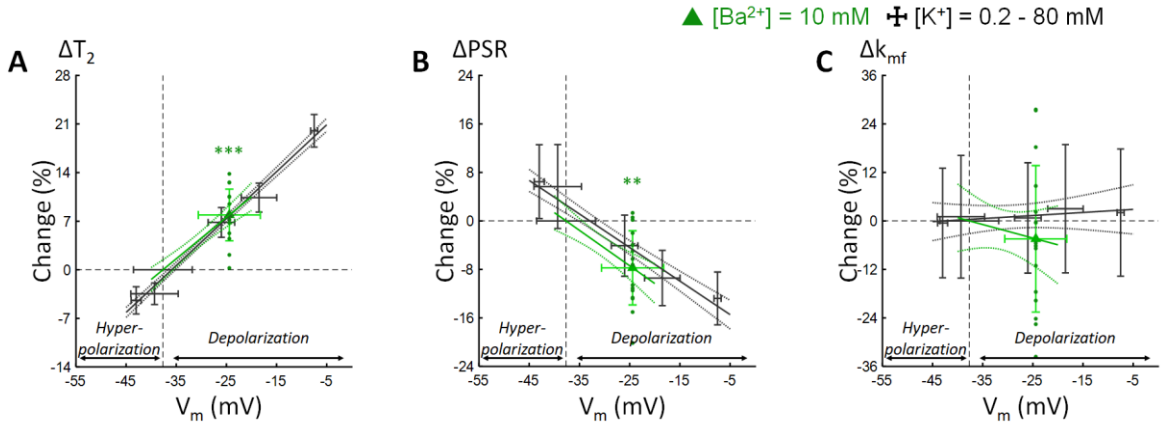

Fig. 3. Comparison of changes in MR parameters of SH-SY5Y cells between two conditions using $[K^+]$ = 0.2–80 mM (gray cross) and $[Ba^{2+}]$ = 10 mM (green triangle), respectively, to manipulate membrane potential (V_m). Changes in (A) T_2, (B) PSR, and (C) k_{mf} are expressed as percentage changes (n = 15) relative to the control condition. Linear regression fits for $[Ba^{2+}]$ data (green line) and $[K^+]$ data (gray line) are presented with 95% confidence intervals. Error bars denote standard deviation. Statistical significance of changes in MR parameters is marked with asterisks (*: $p < 0.05$, **: $p < 0.01$, ***: $p < 0.001$; Bonferroni-corrected).

Using another cell type. To investigate cell type-dependent specificity, we assessed membrane potential-induced changes in MR parameters using a different cell line, Jurkat, under the same experimental conditions as SH-SY5Y (Fig. 1). The extracellular media used to manipulate membrane potential were categorized similarly to the SH-SY5Y experiments: Baseline medium at $[K^+]$ = 4.2 mM; hyperpolarization media at $[K^+]$ = 0.2 and 1 mM; depolarization media at $[K^+]$ = 20, 40, and 80 mM; and depolarization medium at $[Ba^{2+}]$ = 10 mM.

As in the case of SH-SY5Y cells, Jurkat cells exhibited positive changes in T_2 and negative changes in PSR during depolarization. Conversely, during hyperpolarization, changes in T_2 and PSR displayed opposite trend (Fig. 4). For example, during depolarization at the highest $[K^+]$ of 80 mM, T_2 showed a positive change of 15.7 ± 8.6%, whereas PSR showed a negative change of −17.7 ± 11.5%. On the contrary, during hyperpolarization at the lowest $[K^+]$ of 0.2 mM, T_2 showed a negative change of −13.3 ± 7.4%, whereas PSR showed a positive change of 16.6 ± 9.4%.

During the depolarization induced by Ba^{2+} as a K^+ channel blocker ($[Ba^{2+}]$ = 10 mM), changes in T_2 and PSR showed similar patterns to those obtained by varying $[K^+]$ to manipulate membrane potential: T_2 showed a positive change of 9.76 ± 6.92%, while PSR showed a negative change of −11.3 ± 9.3%. In all cases, the change in k_{mf} was not significant. Statistical significance was tested using one-sample t-test (n = 7) with p-values Bonferroni-corrected for the number of comparisons, which was 6.

In summary, the results of Jurkat cells were similar to those of SH-SY5Y cells in terms of the response of MR parameters, such as T_2 and PSR, to membrane potential, except for the degree of change in these MR parameters. Therefore, it is likely that membrane potential-induced changes in these MR parameters are not cell-type specific.

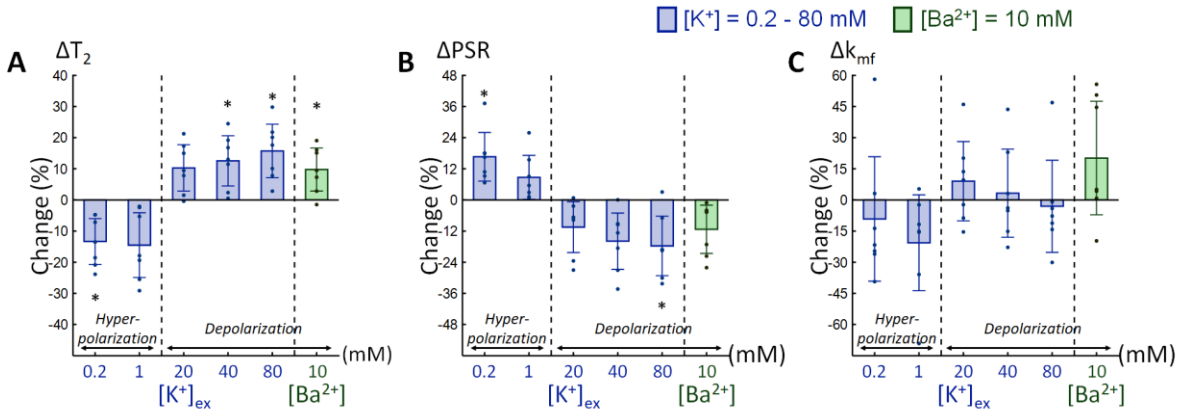

Fig. 4. Changes in MR parameters of Jurkat cells versus extracellular K^+ concentrations ($[K^+]$) and Ba^{2+} concentration ($[Ba^{2+}]$). Changes in (A) T_2, (B) PSR, and (C) k_{mf} are expressed as percentage changes relative to the control condition at $[K^+]$ = 4.2 mM (n = 7). Results are displayed as blue bars for $[K^+]$ and green bars for $[Ba^{2+}]$. Error bars denote standard deviation. Statistical significance of changes in MR parameters is marked with asterisks (*: $p < 0.05$, **: $p < 0.01$, ***: $p < 0.001$; Bonferroni-corrected).

***In vivo* changes in T_2 by membrane potential**

The dependence of MR parameters on membrane potential observed in *in vitro* cell studies was also reproduced in an *in vivo* setting. A craniotomy was performed on rats to expose a 3-mm-diameter region of the cerebral cortex, and the exposed region was perfused with artificial cerebrospinal fluid (aCSF) to modulate the membrane potential (see Methods for more details). During the membrane potential modulation, rats were scanned on the 7 T preclinical MRI system (BioSpec, Bruker) to measure T_2. The experimental setup is presented in Fig. 5. Four experimental conditions were applied sequentially to rats *in vivo* (Fig. 5D): An initial condition using baseline aCSF ($[K^+]$ = 3 mM), depolarization conditions using depolarizing aCSF with $[K^+]$ = 40 and 80 mM, and a recovery condition using baseline aCSF again. Hemodynamics responses were pharmacologically suppressed (see Methods for more details). To assess whether there is an increase in water content due to aCSF perfusion that may significantly contribute to changes in T_2, control experiments were also conducted for the same duration as the four experimental conditions above, using baseline aCSF that does not induce depolarization.

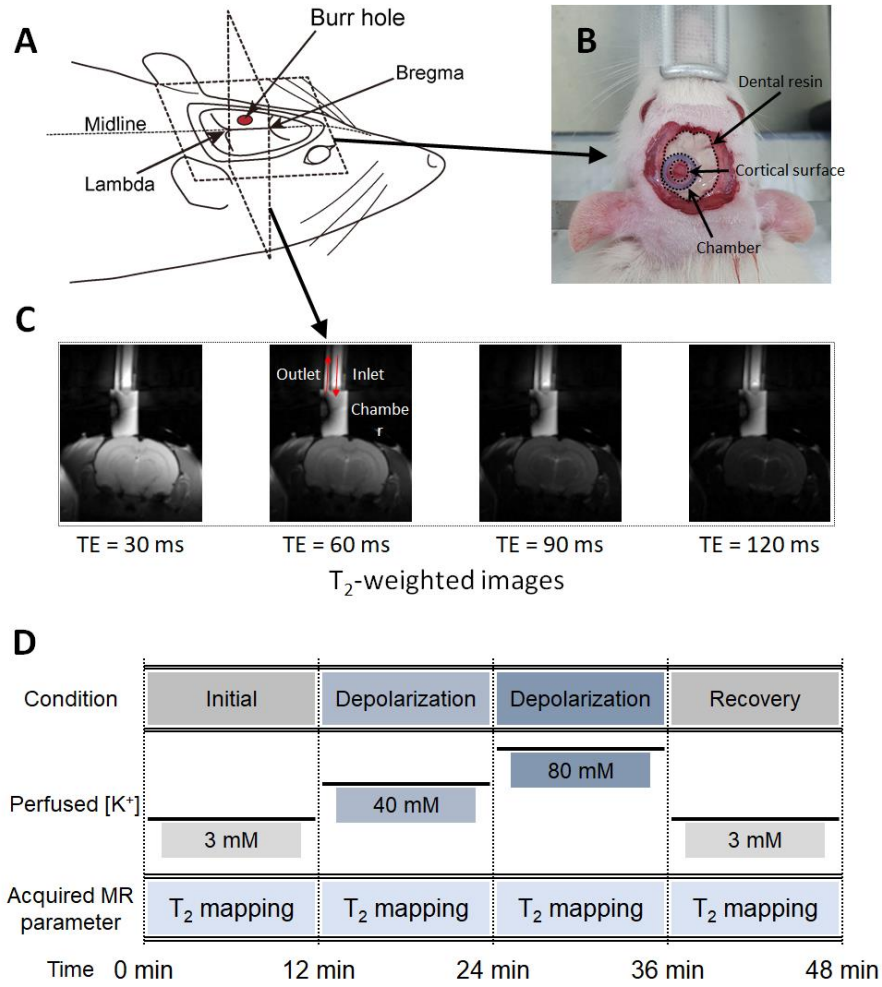

Fig. 5. The experimental setup for *in vivo* manipulation of membrane potential. (A) A schematic diagram of the rat head after a craniotomy. The center of burr hole was located at the coordinates of 2.5 mm anterior and 2.0 mm lateral to the lambda. (B) Photograph of the rat head after fixing a cylindrical chamber on the burr hole. The chamber was filled with the baseline aCSF. (C) A representative series of T_2-weighted MR images for T_2 mapping. The chamber was connected to inlet and outlet perfusion tubes. (D) The

experimental paradigm of rat MR imaging *in vivo*. Four conditions were sequentially applied to each rat: initial, depolarization, further depolarization, and recovery. The T_2 mapping sequence was conducted for 12 minutes during each condition.

In Fig. 6A, T_2 maps from a representative rat depict noticeable increases in T_2 values in regions marked with black arrows during depolarization condition. Changes in T_2 values between different conditions were assessed by defining a ROI containing the perfused cerebral cortex beneath the chamber (Fig. 6B; rectangle, depth = 0.6 mm, width = 1.8 mm). Spatial averaging the signal within the ROI produced a time-course data of T_2 for each rat (Fig. 6C), demonstrating positive changes in T_2 during depolarization and a decrease close to zero during recovery condition. The T_2 change in each condition was compared to the corresponding condition in a control experiment with the same perfusion time but using baseline perfusion aCSF ($[K^+]$ = 3 mM). After 12 minutes from the initial condition, the depolarization condition with $[K^+]$ = 40 mM increased T_2 by 1.4 ± 0.9 % (n = 7). For the control experiment, it was 0.2 ± 0.6% (n = 5). After 24 minutes, the depolarization condition with $[K^+]$ = 80 mM further increased T_2 by 2.3 ± 0.8% (n = 7). In the control experiment, it was 0.5 ± 0.5% (n = 5). The recovery condition reduced the T_2 change back to 0.5 ± 0.1% (n = 2). In the control experiment, it was 0.4 ± 0.5% (n = 5). The T_2 changes in the depolarization condition of $[K^+]$ = 80 mM was statistically significant when compared to the control experiments (two-sample t-test; $[K^+]$ = 40 mM, $p > 0.05$; $[K^+]$ = 80 mM, $p < 0.01$; Bonferroni-corrected for the number of comparisons = 2). Our observations demonstrate that *in vivo* manipulation of membrane potential shows similar trends to *in vitro* cell experiments. However, the magnitude of T_2 changes in rat cerebral cortex *in vivo* was smaller than those in SH-SY5Y cells *in vitro*. This difference may be mainly due to the incomplete replacement of extracellular fluid to perfused aCSF within the ROI of the imaging slice. This might result from limited diffusion of aCSF through leptomeninges[29,30] and the constant removal of excessive K^+ through clearing mechanism[31,32]. Consequently, the actual $[K^+]$ may be lower than the designated $[K^+]$ of the extracellular fluid, leading to smaller membrane potential changes. The difference in cell types between SH-SY5Y cells *in vitro* and rat cerebral cortex cells *in vivo* could also contribute to the observed differences between *in-vivo* and *in-vitro* results. For the detailed analysis on the quality of T2 mapping, refer to Supplementary Section S3.1, Fig. S6, and Table S4.

Voxel-wise statistical analysis was also performed using two-sample t-test between T_2 maps of $[K^+]$ = 80 mM and 3 mM. The resulting t-value map in Fig. 6D, displayed with a threshold of $p < 0.05$ and a cluster size ≥ 5, indicates significant changes in T_2 within the perfused cortex region below the chamber. Unlike previous MRI studies, which utilized high $[K^+] \geq 1$ M and reported spreading depression induced by depolarization in a craniotomy-exposed cortex[33,34], spreading depression was not observed here, which may be due to the use of significantly lower $[K^+] \leq 80$ mM in this study.

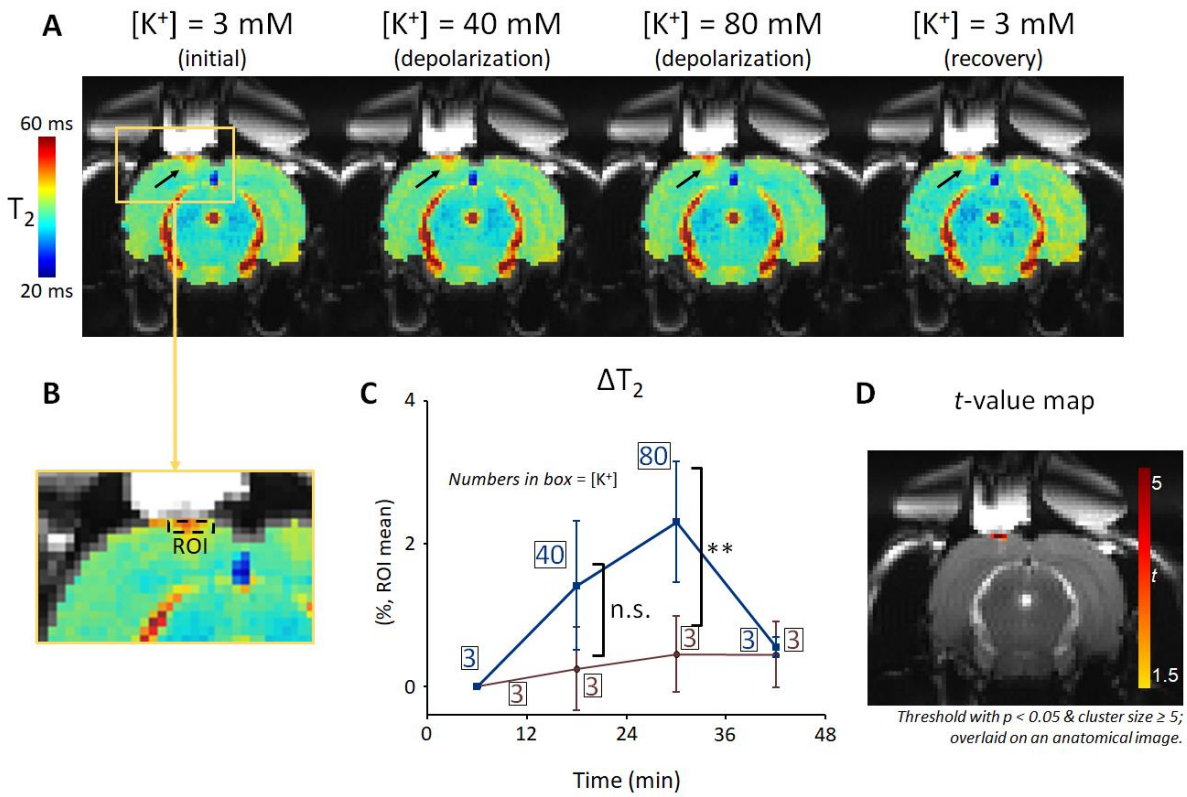

Fig. 6. *In vivo* T_2 mapping results in rat models. (A) Representative T_2 mapping results from a single rat during control, depolarization, and recovery conditions. Regions showing T_2 changes are marked with black arrows. (B) The ROI for T_2 change evaluation is marked by a black dashed rectangle (depth = 0.6 mm, width = 1.8 mm). (C) T_2 averaged within an ROI and expressed as percentage changes relative to the initial condition with $[K^+]$ = 3 mM. The blue line with square markers represents the experiments involving $[K^+]$ changes in perfused aCSF, and the brown line with round markers represents the control experiments involving no $[K^+]$ changes in perfused aCSF. The numbers in boxes represents $[K^+]$ of perfused aCSF. Statistical significance was tested using two-sample t-test (n.s.: $p > 0.05$, **: $p < 0.01$; Bonferroni-corrected). (D) The voxel-wise t-value map, overlaid on the T_2-weighted MR image with a threshold of $p < 0.05$ and a cluster size ≥ 5 within the brain mask. The t-value map resulted from a two-sample t-test between T_2 maps obtained with the depolarization condition of $[K^+]$ = 80 mM and the control condition of $[K^+]$ = 3 mM.

Discussion

In this study, our results demonstrate that changes in membrane potential can be detected through changes in MR parameters, specifically T_2 relaxation time and pool size ratio (PSR). We conducted experiments using cultured cells *in vitro* as well as rat models *in vivo*. *In vitro* cell experiments were designed to obtain results without physiological factors such as hemodynamic responses and respiration, which may become confounding factors *in vivo*. When the membrane potential of cultured cells *in vitro* was depolarized (or hyperpolarized), T_2 increased (or decreased) and PSR decreased (or increased). *In vivo* experiments involved pharmacological suppression of hemodynamic responses to minimize their effects on T_2. The *in vivo* experiments showed a consistent trend with the *in vitro* experiments in the dependence of T_2 on membrane potential, i.e., increase in T_2 during depolarization. However, the change in T_2 induced by

depolarization (~3%) was approximately one-fifth of the change observed in SH-SY5Y cells *in vitro* (~15%).

Several factors may contribute to differences between in-vivo and in-vitro results. First, in the *in vivo* setting, the actual extracellular K^+ concentration ($[K^+]$) experienced by cortical cells may be lower than the $[K^+]$ of perfused aCSF. One reason for the reduction in the actual $[K^+]$ experienced by cortical cells is the membranes between the skull and cortex. For example, even with the removal of dura mater, the depolarizing aCSF should diffuse through leptomeninges, which can be a limiting factor[29,30]. Moreover, constant removal of excessive K^+ by clearing mechanisms[31,32] may further reduce the actual extracellular $[K^+]$ experienced by perfused cells. Lastly, differences in cell types between *in-vitro* and *in-vivo* experiments may also contribute to the observed discrepancies between them. Partial volume effects, also related to the spatial dependence of perfusion $[K^+]$ in the cortex, may be another cause of the observed differences between *in-vivo* and *in-vitro* results.

Our findings reveal that the T_2 relaxation time as well as magnetization transfer (MT) directly reflect changes in membrane potential, carrying significant implications from biophysical and neuroscientific perspectives. In particular, the correlation between PSR and membrane potential suggests a potential link between T_2 changes and hydration water on the cell membrane. This inference arises from interpreting a change in PSR as a change in the density of hydration water, which partially belongs to a macromolecular pool[35]. A recent study utilizing optical measurements demonstrated a decrease in neuronal membrane hydration water during depolarization[36]. Additionally, MR studies have also shown that hydration water has a significantly shorter T_2 than bulk water due to its slower re-orientational and diffusive motions[37]. Integrating the previous studies with our observations, depolarization may reduce the density of hydration water on the cell membrane, resulting in a decrease in PSR and an increase in T_2. Conversely, hyperpolarization appears to increase the density of hydration water on the cell membrane, increasing PSR and decreasing T_2.

Another potential mechanism underlying membrane potential-induced changes in MR parameters involves cell swelling or shrinking. Depolarization (or hyperpolarization) of the membrane potential can lead to cell swelling (or shrinking)[38-40]. This correlation between cell volume and membrane potential suggests that changes in MR parameters may be attributed to alterations in cellular volume, affecting the amount of cellular content per unit volume. Notably, neuronal or glial cell swelling has been proposed as one of the candidate mechanisms of diffusion fMRI[41-43].

In addition, these findings provide important insights into the underlying contrast mechanism of the recently proposed DIANA technique[24], whose signal directly correlates with neuronal activity but remains unexplained by neuronal current models[16]. Admittedly, our experimental paradigm is based on clamping the membrane potential at a specific level, thus measuring changes in T_2 and PSR during static depolarization or hyperpolarization rather than time-varying membrane potentials (e.g., action potential in neurons). Future research directions may involve validating our results under conditions of temporally varying membrane potential, such as during action potentials. Large invertebrate neurons, such as those from *Aplysia*, may serve as suitable model systems for such investigations. Simultaneous electrode recording would be useful to evaluate the temporal correlation between membrane potential changes and MR parameters. These experiments hold the potential to assess the feasibility of MRI in imaging neural activity by detecting changes in membrane potential.

Some experimental imperfections and limitations need to be discussed in this study. Firstly, maintaining *in vitro* cells in the desired environment (37°C and 5% CO_2), particularly during MRI scans, can be challenging. Another concern regarding the desired extracellular environment is related to the Ba^{2+}-

induced depolarization experiment, where intracellular accumulation of Ba^{2+} may significantly impact cellular integrity. However, literature suggests that the Ba^{2+}-current entering the cytoplasm exponentially decays[44,45], thereby potentially limiting intracellular [Ba^{2+}][46-48]. To address these concerns about cellular integrity, cell viability assays were performed on SH-SY5Y cells to confirm viability under a fluorescent microscope using Calcein AM and EthD-1 staining. In all cases, cell viability was greater than 97.6% (see the Supplementary information). Secondly, the potential impact of distinct T_2 values in each extracellular medium on T_2 measurements for cells necessitates consideration of the partial volume effect. However, in this study, the differences in T_2 among the extracellular media were found to be negligible when compared to the observed T_2 changes (see the Supplementary information, Fig S2). Thirdly, while our findings demonstrate the possibility of detecting changes in membrane potential using MR contrast, it is important to note that our approach may not be applicable for measuring the absolute value of membrane potential. Finally, changes in T_2 and magnetization transfer can arise from sources other than membrane potential alone. Factors such as pH, energy depletion, or extracellular osmolarity can influence cell volume, which in turn affects MR parameters. Therefore, distinguishing the effect of membrane potential from other volume-altering factors could be challenging.

In addition to the presented T_2 measurements, T_1 measurements were also conducted for reference and are presented in the Supplementary information. The observed changes in T_1 were approximately 3 to 6 times lower than those in T_2, indicating that T_2 is much more sensitive to membrane potential than T_1.

In summary, our study demonstrates that MR parameters, such as T_2 and PSR, can reflect changes in membrane potential both *in vitro* and *in vivo*. This observation introduces a pioneering approach for noninvasively detecting changes in membrane potential using MRI.

Methods

In vitro cell culture

An immortalized human neuroblastoma cell line, SH-SY5Y, was purchased from the American Type Culture Collection (ATCC) and cultured in DMEM/F12 containing 10% (v/v) fetal bovine serum and 100 U/ml penicillin/streptomycin at 37°C and 5% CO_2. A human leukemia cell line, Jurkat, was also purchased from the ATCC. It was cultured in RPMI-1640 containing 10% (v/v) fetal bovine serum and 100 U/ml penicillin/streptomycin at 37°C and 5% CO_2.

In vitro manipulation of membrane potential with extracellular media

The baseline extracellular medium was prepared with the following components: KCl = 4.2 mM; NaCl = 145.8 mM; HEPES = 20 mM; glucose = 4.5 g/l; EGTA = 10 µM; pH = 7.2. This baseline medium was considered a control condition for various extracellular media used to adjust membrane potential. Two extracellular media with low K^+ concentrations (KCl = 0.2 and 1 mM) were prepared to hyperpolarize the membrane potential. Three extracellular media with high K^+ concentrations (KCl = 20, 40, and 80 mM) were prepared to depolarize the membrane potential. A Ba^{2+} medium containing 10 mM $BaCl_2$ was also prepared to depolarize the membrane potential in a different way, i.e., as a K^+ channel blocker. These seven extracellular media were used for both MR imaging and patch clamp recording *in vitro*. Sodium ion concentrations ([Na^+]) in all media were controlled to match the osmolarity with the baseline medium. The composition of all extracellular media is detailed in the Supplementary information.

Preparation of cells for *in vitro* MR measurement

SH-SY5Y cells were harvested and concentrated into a pellet (~70 µl) by centrifugation at 250 × g for 2 min. The pellet was resuspended in the culture medium and divided evenly into seven aliquots. Each cell suspension was centrifuged and resuspended in each of the seven different media specified in Table S1. Centrifugation and resuspension were repeated three more times to completely clear out the culture medium. Each cell suspension with a different extracellular medium was then loaded into two wells on the same column of an acrylic container with 14 wells (matrix = 2 × 7) and centrifuged again to concentrate into pellets (Fig. 1). The acrylic container was purposely formed into a spherical segment to enhance the homogeneity of the static magnetic field[49]. The preparation of Jurkat cell samples was the same as for the SH-SY5Y cell samples.

In vitro MRI experiment

In vitro MRI experiments were performed on a 9.4 T MRI system (BioSpec 94/30 USR, Bruker BioSpin) at room temperature. A volume coil with an inner diameter of 86 mm was utilized for both radiofrequency (RF) pulse transmission and signal reception. Within the acrylic container, two wells on the same column (matrix = 2 × 7) contained identical cell pellets with the same extracellular media. MRI signals from seven different cell samples in the horizontal direction were separated by one-dimensional frequency encoding along that direction (Fig. 1). The MRI pulse sequence employed for mapping the T_2 value was a single-echo spin-echo (SSE) sequence with 50 variable echo times (TE) spaced between 9.5 and 290.5 ms on a logarithmic scale. For mapping the quantitative magnetization transfer (qMT), an inversion recovery multi-echo spin-echo (IR-MSE) sequence was used. The inversion times (TI) for the IR-MSE sequence were optimized using the theory of Cramér-Rao lower bounds[50]. The optimized TIs ranged from 4 to 10,079.4 ms. After each TI, 16 spin-echo trains were acquired with an echo spacing of 9.5 ms. Total scan time for both sequences was 23 minutes. Experiments were repeated 15 times for SH-SY5Y cells and 7 times for Jurkat cells, replacing cells in each repetition. Other scan parameters are detailed in the Supplementary information.

Animals

Male Wistar rats aged 8 weeks (250–300 g, Orient Bio) were used for MRI experiments after undergoing a craniotomy. All animal experiments were approved by the Institutional Animal Care and Use Committee at the National Cancer Center Korea (NCC-22-740). The rats were housed in ventilated cages under a 12h/12h light/dark cycle and provided with *ad libitum* access to food and water.

In vivo manipulation of membrane potential with artificial cerebrospinal fluid (aCSF)

The membrane potential of the exposed cortex was manipulated by directly perfusing the region-of-interest of the cerebral cortex with aCSF after a craniotomy. The baseline aCSF was prepared with the following components: KCl = 3 mM; NaCl = 135 mM; $MgCl_2$ = 3 mM; HEPES = 20 mM; glucose = 4.5 g/l; EGTA = 2 mM; N_ω-Nitro-L-arginine = 1 mM; Nifedipine = 0.1 mM; pH = 7.4. Hemodynamic effects were pharmacologically suppressed using N_ω-Nitro-L-arginine, Nifedipine, and EGTA. N_ω-Nitro-L-arginine suppresses depolarization-induced hemodynamic response by blocking the synthesis of nitric

oxide, which acts as a vasodilator[51]. Nifedipine blocks voltage-sensitive Ca^{2+} channels, and EGTA chelates free Ca^{2+} to inhibit the hemodynamic response[52]. To induce depolarization, aCSF with high $[K^+]$ (KCl = 40 and 80 mM) was prepared. The osmolarity of the aCSF was matched with the concentration of NaCl.

Rat surgery

A craniotomy was performed on a Wistar rat. The experimental setup after a surgical procedure is illustrated in Fig. 5. The surgery was performed following an established protocol[53]. Anesthesia was induced with 3% isoflurane in O_2 and maintained with 2–3% isoflurane during the surgical procedure. Body temperature was maintained at 36.5–37.5°C with an infrared lamp. The head was fixed with a small animal stereotaxic frame. The hair on the scalp was shaved with a veterinary clipper. The skin and periosteum over the skull were removed using a scalpel and surgical scissors. A 3.0-mm-diameter burr hole was opened using a dental drill with its center at the coordinates of 2.5 mm anterior and 2.0 mm lateral to the lambda. Then, a cylindrical chamber was implanted upon the burr hole with cyanoacrylate glue and dental composite resin. The chamber was filled with the baseline aCSF and connected to inlet and outlet perfusion tubes. The exposed cerebral cortex inside the chamber was perfused with the baseline aCSF at a flow rate of 0.6 ml/min using peristaltic pumps.

***In vivo* MRI experiment**

The rat with a cranial chamber installed on the cortical surface was placed on a 7 T MRI system (BioSpec 70/20 USR, Bruker BioSpin), fixed in a customized cradle with two ear-bars and a bite-bar. A customized surface coil (rectangular, 35 mm × 20 mm) was used for RF pulse transmission and signal reception. Body temperature was maintained at 36.5–37.5°C using a warm air blower. Anesthesia was maintained with 2% isoflurane in O_2 (0.6 l/min). Respiration rate and body temperature were monitored throughout the MRI experiment. MR images were acquired in a 2 mm coronal slice through the center of the burr hole (Fig. 5C). For T_2 mapping, a multi-echo spin-echo (MSE) sequence with 20 TEs (7.5 to 150 ms) was used. Other scan parameters are detailed in the Supplementary information.

Rats were sequentially subjected to four experimental conditions, as depicted in Fig. 5D. First, the exposed cerebral cortex was perfused with baseline aCSF ($[K^+]$ = 3 mM) as the control condition. Second, as a depolarizing condition, the perfusion media was switched to depolarizing aCSF of $[K^+]$ = 40 mM. Third, membrane potential was further depolarized by perfusion with aCSF of $[K^+]$ = 80 mM. Finally, as a recovery condition, the perfusion media was changed back to baseline aCSF. During each condition, MR images were acquired with MSE sequences for 12 minutes. The experiment was repeated for seven rats. Two rats underwent the whole four conditions, while other five rats underwent the same conditions except for the recovery condition. As a control experiment, another set of rats (n = 5) underwent perfusion with the baseline aCSF for the same duration (48 minutes) as the previous experiment, and MR images were acquired with four MSE sequences, each for 12 minutes. Throughout the experiment, the perfusion rate was maintained at 0.6 ml/min.

Quantification of MR parameters

For the *in vivo* MR images acquired with a MSE sequence, echo trains were matched with a simulated dictionary of decay curves of multi-echo spin-echo signals created with the stimulated echo and

slice profile correction[54] to estimate T_2 values. For the *in vitro* one-dimensional MR images acquired with the SSE sequence, signals were fitted to a mono-exponential function to estimate T_2 values. For the *in vitro* one-dimensional MR images acquired with the IR-MSE sequence, signals were fitted to a bi-exponential function[55,56] to estimate qMT. 16 spin echoes acquired after each TI were averaged to improve SNR. The qMT parameters such as PSR and k_{mf} were derived from this fitting process. For the detailed procedure to calculate T_2 and two qMT parameters (i.e., PSR and k_{mf}), see the Supplementary information.

Patch clamp recordings

The membrane potential of SH-SY5Y cells was recorded at room temperature using the whole-cell mode of the patch clamp technique[57]. The bath solution was the same as the extracellular medium used in the MRI experiment and was constantly perfused at a flow rate of 2 ml/min. The composition of the pipette solution was as follows: KCl = 140 mM; NaCl = 5 mM; MgCl2 = 3 mM; HEPES = 10 mM; Mg-ATP = 1 mM; Na-GTP = 0.5 mM. The pH of the pipette solution was adjusted to 7.4 using KOH. Calcium ions (Ca^{2+}) were not included in the pipette solution to minimize Ca^{2+}-dependent currents. The resistance of the electrode was 3–5 MΩ with the internal solution filled. Recordings were performed with a patch amplifier (Axopatch-1D; Axon Instruments) and a current clamp was also used to monitor the membrane potential. The experiment was repeated three times, with cells replaced at each repetition.

Acknowledgements

We thank Dr. Silvia Mangia for insightful discussions on the role of hydration water in functional MRI. Animal molecular imaging facility at the National Cancer Center Korea contributed for supportive animal magnetic resonance imaging. We thank Minsun Kim and Soyeon Jeon (National Cancer Center) for helping with rat craniotomies and MRI experiments. This work was supported by the National Research Foundation of Korea grant funded by the Ministry of Science and ICT (NRF-2019M3C7A1031993, NRF-2019M3C7A1031994, and NRF-2023R1A2C3007075). This work was supported by the Commercialization Promotion Agency for R&D Outcomes (COMPA) funded by the Ministry of Science and ICT (NTIS1711198890).

Author contributions

Conceptualization: K.M., S.-K.L., and J.-Y.P. **Methodology**: K.M., S.C., S.-K.L., J.L., P.T.T., D.K., J.S.L., and J.-Y.P. **Investigation**: K.M., S.C., P.T.T., and D.K.; **Resources**: S.C., J.L., D.K., J.S.L., and J.-Y.P. **Visualization**: K.M., and S.C. **Supervision**: J.L., and J.-Y.P. **Writing – original draft** K.M., and J.-Y.P. **Writing – review & editing**: K.M., S.C., S.-K.L., J.L., P.T.T., D.K., J.S.L., and J.-Y.P.

Declaration of interests

The authors declare no competing interests.

Resource availability

Lead contact

Further information and requests for resources and reagents should be directed to and will be fulfilled by the lead contact, Jang-Yeon Park (jyparu@skku.edu).

Materials availability

This study did not generate new unique reagents.

Data and code availability

· All original data reported in this paper will be shared by the lead contact upon request.

· This paper does not report original code.

· Any additional information required to reanalyze the data reported in this work is available from the lead contact upon request.

References

1. Abdul Kadir, L., Stacey, M., and Barrett-Jolley, R. (2018). Emerging roles of the membrane potential: Action beyond the action potential. Frontiers in Physiology *9*, 1661. https://doi.org/10.3389/fphys.2018.01661.
2. Jefferys, J.G.R. (1995). Nonsynaptic modulation of neuronal activity in the brain: Electric currents and extracellular ions. Physiological Reviews *75*, 689-723. https://doi.org/10.1152/physrev.1995.75.4.689.
3. Helfant, R.H. (1986). Hypokalemia and arrhythmias. The American Journal of Medicine *80*, 13-22. https://doi.org/10.1016/0002-9343(86)90336-0.
4. Kane, C., Shepherd, R.M., Squires, P.E., Johnson, P.R.V., James, R.F.L., Milla, P.J., Aynsley-Green, A., Lindley, K.J., and Dunne, M.J. (1996). Loss of functional K_{ATP} channels in pancreatic β-cells causes persistent hyperinsulinemic hypoglycemia of infancy. Nature Medicine *2*, 1344-1347. https://doi.org/10.1038/nm1296-1344.
5. Ling, G., and Gerard, R.W. (1949). The normal membrane potential of frog sartorius fibers. Journal of Cellular and Comparative Physiology *34*, 383-396. https://doi.org/10.1002/jcp.1030340304.
6. Neher, E., and Sakmann, B. (1976). Single-channel currents recorded from membrane of denervated frog muscle fibres. Nature *260*, 799-802. https://doi.org/10.1038/260799a0.
7. Tasaki, I., Watanabe, A., Sandlin, R., and Carnay, L. (1968). Changes in fluorescence, turbidity, and birefringence associated with nerve excitation. P Natl Acad Sci USA *61*, 883-888. https://doi.org/10.1073/pnas.61.3.883.
8. Tsien, R.Y. (1980). New calcium indicators and buffers with high selectivity against magnesium and protons: Design, synthesis, and properties of prototype structures. Biochemistry-Us *19*, 2396-2404. https://doi.org/10.1021/bi00552a018.
9. Zhou, Y., Liu, E., Müller, H., and Cui, B. (2021). Optical electrophysiology: Toward the goal of label-free voltage imaging. J Am Chem Soc *143*, 10482-10499. https://doi.org/10.1021/jacs.1c02960.
10. Berger, H. (1929). Über das elektrenkephalogramm des menschen. Archiv für Psychiatrie und Nervenkrankheiten *87*, 527-570. https://doi.org/10.1007/BF01797193.
11. Cohen, D. (1968). Magnetoencephalography: Evidence of magnetic fields produced by alpha-rhythm currents. Science *161*, 784-786. https://doi.org/10.1126/science.161.3843.784.
12. Mansfield, P. (1977). Multi-planar image formation using NMR spin echoes. Journal of Physics C: Solid State Physics *10*, L55-L58. https://doi.org/10.1088/0022-3719/10/3/004.

13. He, B., Sohrabpour, A., Brown, E., and Liu, Z. (2018). Electrophysiological source imaging: A noninvasive window to brain dynamics. Annu Rev Biomed Eng *20*, 171-196. https://doi.org/10.1146/annurev-bioeng-062117-120853.
14. Ogawa, S., Lee, T.-M., Nayak, A.S., and Glynn, P. (1990). Oxygenation-sensitive contrast in magnetic resonance image of rodent brain at high magnetic fields. Magnetic Resonanace in Medicine *14*, 68-78. https://doi.org/10.1002/mrm.1910140108.
15. Logothetis, N.K., Pauls, J., Augath, M., Trinath, T., and Oeltermann, A. (2001). Neurophysiological investigation of the basis of the fMRI signal. Nature *412*, 150-157. https://doi.org/10.1038/35084005.
16. Roth, B.J. (2023). Can MRI be used as a sensor to record neural activity? Sensors *23*, 1337. https://doi.org/10.3390/s23031337.
17. Bodurka, J., and Bandettini, P.A. (2002). Toward direct mapping of neuronal activity: MRI detection of ultraweak, transient magnetic fields changes. Magnet Reson Med *47*, 1052-1058. https://doi.org/10.1002/mrm.10159.
18. Konn, D., Gowland, P., and Bowtell, R. (2003). MRI detection of weak magnetic fields due to an extended current dipole in a conducting sphere: A model for direct detection of neuronal currents in the brain. Magnet Reson Med *50*, 40-49. https://doi.org/10.1002/mrm.10494.
19. Chow, L.S., Cook, G.G., Whitby, E., and Paley, M.N.J. (2006). Investigating direct detection of axon firing in the adult human optic nerve using MRI. NeuroImage *30*, 835-846. https://doi.org/10.1016/j.neuroimage.2005.10.024.
20. Xiong, J., Fox, P.T., and Gao, J.-H. (2003). Directly mapping magnetic field effects of neuronal activity by magnetic resonance imaging. Human Brain Mapping *20*, 41-49. https://doi.org/10.1002/hbm.10124.
21. Chu, R., de Zwart, J.A., van Gelderen, P., Fukunaga, M., Kellman, P., Holroyd, T., and Duyn, J.H. (2004). Hunting for neuronal currents: Absence of rapid MRI signal changes during visual-evoked response. NeuroImage *23*, 1059-1067. https://doi.org/10.1016/j.neuroimage.2004.07.003.
22. Luo, Q., Lu, H., Lu, H., Senseman, D., Worsley, K., Yang, Y., and Gao, J.-H. (2009). Physiologically evoked neuronal current MRI in a bloodless turtle brain: Detectable or not? NeuroImage *47*, 1268-1276. https://doi.org/10.1016/j.neuroimage.2009.06.017.
23. Parkes, L.M., de Lange, F.P., Fries, P., Toni, I., and Norris, D.G. (2007). Inability to directly detect magnetic field changes associated with neuronal activity. Magnet Reson Med *57*, 411-416. https://doi.org/10.1002/mrm.21129.
24. Toi, P.T., Jang, H.J., Min, K., Kim, S.-P., Lee, S.-K., Lee, J., Kwag, J., and Park, J.-Y. (2022). In vivo direct imaging of neuronal activity at high temporospatial resolution. Science *378*, 160-168. https://doi.org/10.1126/science.abh4340.
25. Lesage, F., and Lazdunski, M. (2000). Molecular and functional properties of two-pore-domain potassium channels. American Journal of Physiology: Renal Physiology *279*, F793-F801. https://doi.org/10.1152/ajprenal.2000.279.5.F793.
26. Ma, X.-Y., Yu, J.-M., Zhang, S.-Z., Liu, X.-Y., Wu, B.-H., Wei, X.-L., Yan, J.-Q., Sun, H.-L., Yan, H.-T., and Zheng, J.-Q. (2011). External Ba^{2+} block of the two-pore domain potassium channel TREK-1 defines conformational transition in its selectivity filter. Journal of Biological Chemistry *286*, 39813-39822. https://doi.org/10.1074/jbc.M111.264788.
27. Vaughan, P.F.T., Kaye, D.F., Ball, S.G., Reeve, H.L., and Peers, C. (1995). The effect of barium on [^{3}H]noradrenalin release from the human neuroblastoma SH-SY5Y. European Journal of Neuroscience *7*, 875-880. https://doi.org/10.1111/j.1460-9568.1995.tb01074.x.
28. Pottosin, I.I., Bonales-Alatorre, E., Valencia-Cruz, G., Mendoza-Magaña, M.L., and Dobrovinskaya, O.R. (2008). TRESK-like potassium channels in leukemic T cells. Pflügers Archiv *456*, 1037-1048. https://doi.org/10.1007/s00424-008-0481-x.
29. Chung, S., Jung, W., and Lee, M.-Y. (1999). Inward and outward rectifying potassium currents set membrane potentials in activated rat microglia. Neuroscience Letters *262*, 121-124. https://doi.org/10.1016/S0304-3940(99)00053-1.

30. Bradbury, M.W.B., Segal, M.B., and Wilson, J. (1972). Transport of potassium at the blood-brain barrier. Journal of Physiology *221*, 617-632. https://doi.org/10.1113/jphysiol.1972.sp009771.
31. Filippidis, A.S., Zarogiannis, S.G., Ioannou, M., Gourgoulianis, K., Molyvdas, P.-A., and Hatzoglou, C. (2012). Permeability of the arachnoid and pia mater. The role of ion channels in the leptomeningeal physiology. Child's Nervous System *28*, 533-540. https://doi.org/10.1007/s00381-012-1688-x.
32. Walz, W. (2000). Role of astrocytes in the clearance of excess extracellular potassium. Neurochemistry International *36*, 291-300. https://doi.org/10.1016/S0197-0186(99)00137-0.
33. O'Donnell, M.E. (2009). Ion and Water Transport across the Blood-Brain Barrier. In Physiology and Pathology of Chloride Transporters and Channels in the Nervous System, F.J. Alvarez-Leefmans, and E. Delpire, eds. (Academic Press), pp. 585-606. https://doi.org/10.1016/B978-0-12-374373-2.00030-3.
34. Stanisz, G.J., Yoon, R.S., Joy, M.L.G., and Henkelman, R.M. (2002). Why does MTR change with neuronal depolarization? Magnet Reson Med *47*, 472-475. https://doi.org/10.1002/mrm.10071.
35. Autio, J.A., Shatillo, A., Giniatullin, R., and Gröhn, O.H. (2014). Parenchymal spin-lock fMRI signals associated with cortical spreading depression. Journal of Cerebral Blood Flow & Metabolism *34*, 768-775. https://doi.org/10.1038/jcbfm.2014.16.
36. Hazlewood, C.F., Chang, D.C., Nichols, B.L., and Woessner, D.E. (1974). Nuclear magnetic resonance transverse relaxation times of water protons in skeletal muscle. Biophysical Journal *14*, 583-606. https://doi.org/10.1016/S0006-3495(74)85937-0.
37. Didier, M.E.P., Tarun, O.B., Jourdain, P., Magistretti, P., and Roke, S. (2018). Membrane water for probing neuronal membrane potentials and ionic fluxes at the single cell level. Nature Communications *9*, 5287. https://doi.org/10.1038/s41467-018-07713-w.
38. Mathur-De Vré, R. (1980). The NMR Studies of water in biological systems. Progress in Biophysics and Molecular Biology *35*, 103-134. https://doi.org/10.1016/0079-6107(80)90004-8.
39. Lang, F., Busch, G.L., Ritter, M., Völkl, H., Waldegger, S., Gulbins, E., and Häussinger, D. (1998). Functional significance of cell volume regulatory mechanisms. Physiological Reviews *78*, 247-306. https://doi.org/10.1152/physrev.1998.78.1.247.
40. Mangia, S., Chamberlain, R., De Martino, F., Moeller, S., Corum, C., Kim, T., Kalavagunta, C., Michaeli, S., Garwood, M., Kim, S.-G., and Ugurbil, K. (2012). Functional MRI with SWIFT. Proceedings of International Society of Magnetic Resonance in Medicine *20*, 0326.
41. Fraser, J.A., and Huang, C.L.-H. (2004). A quantitative analysis of cell volume and resting potential determination and regulation in excitable cells. Journal of Physiology *559*, 459-478. https://doi.org/10.1113/jphysiol.2004.065706.
42. Hoffmann, E.K., Lambert, I.H., and Pedersen, S.F. (2009). Physiology of cell volume regulation in vertebrates. Physiological Reviews *89*, 193-277. https://doi.org/10.1152/physrev.00037.2007.
43. Le Bihan, D., Urayama, S.-i., Aso, T., Hanakawa, T., and Fukuyama, H. (2006). Direct and fast detection of neuronal activation in the human brain with diffusion MRI. P Natl Acad Sci USA *103*, 8263-8268. https://doi.org/10.1073/pnas.0600644103.
44. Le Bihan, D. (2012). Diffusion, confusion and functional MRI. NeuroImage *62*, 1131-1136. https://doi.org/10.1016/j.neuroimage.2011.09.058.
45. Mashimo, S., Kuwabara, S., Yagihara, S., and Higasi, K. (1987). Dielectric relaxation time and structure of bound water in biological materials. J Phys Chem-Us *91*, 6337-6338. https://doi.org/10.1021/j100309a005.
46. Nandi, N., and Bagchi, B. (1997). Dielectric relaxation of biological water. Journal of Physical Chemistry B *101*, 10954-10961. https://doi.org/10.1021/jp971879g.
47. Ferreira, G., Yi, J., Ríos, E., and Shirokov, R. (1997). Ion-dependent inactivation of barium current through L-type calcium channels Journal of General Physiology *109*, 449-461. https://doi.org/10.1085/jgp.109.4.449.

48. Findlay, I. (2002). Voltage- and cation-dependent inactivation of L-type Ca^{2+} channel currents in guinea-pig ventricular myocytes. Journal of Physiology *541*, 731-740. https://doi.org/10.1113/jphysiol.2002.019729.
49. Zhang, B.-X., Zhao, H., Loessberg, P.A., and Muallem, S. (1992). Regulation of agonist-evoked $[Ca^{2+}]_i$ oscillation by intracellular Ca^{2+} and Ba^{2+} in AR42J cells. American Journal of Physiology: Cell Physiology *262*, C1125-C1133. https://doi.org/10.1152/ajpcell.1992.262.5.C1125.
50. Liu, Y.-J., Grapengiesser, E., Gylfe, E., and Hellman, B. (1994). Glucose-induced oscillations of Ba^{2+} in pancreatic β-cells occur without involvement of intracellular mobilization. Archives of Biochemistry and Biophysics *315*, 387-392. https://doi.org/10.1006/abbi.1994.1515.
51. Thomas, R.C. (2009). The plasma membrane calcium ATPase (PMCA) of neurones is electroneutral and exchanges 2 H^+ for each Ca^{2+} or B^{a2}+ ion extruded. Journal of Physiology *587*, 315-327. https://doi.org/10.1113/jphysiol.2008.162453.
52. Lee, S.-H., Han, M.-J., Lee, J., and Lee, S.-K. (2020). Experimental setup for bulk susceptibility effect-minimized, multi-orientation MRI of *ex vivo* tissue samples. Medical Physics *47*, 3032-3043. https://doi.org/10.1002/mp.14174.
53. Li, K., Zu, Z., Xu, J., Janve, V.A., Gore, J.C., Does, M.D., and Gochberg, D.F. (2010). Optimized inversion recovery sequences for quantitative T_1 and magnetization transfer imaging. Magnetic Resonanace in Medicine *64*, 491-500. https://doi.org/10.1002/mrm.22440.
54. Dreier, J.P., Körner, K., Görner, A., Lindauer, U., Weih, M., Villringer, A., and Dirnagl, U. (1995). Nitric oxide modulates the CBF response to increased extracellular potassium. J Cerebr Blood F Met *15*, 914-919. https://doi.org/10.1038/jcbfm.1995.116.
55. Redmond, L., Kashani, A.H., and Ghosh, A. (2002). Calcium regulation of dendritic growth via CaM kinase IV and CREB-mediated transcription. Neuron *34*, 999-1010. https://doi.org/10.1016/s0896-6273(02)00737-7.
56. Mostany, R., and Portera-Cailliau, C. (2008). A craniotomy surgery procedure for chronic brain imaging. Journal of Visualized Experiments, e680. https://doi.org/10.3791/680.
57. McPhee, K.C., and Wilman, A.H. (2017). Transverse relaxation and flip angle mapping: Evaluation of simultaneous and independent methods using multiple spin echoes. Magnet Reson Med *77*, 2057-2065. https://doi.org/10.1002/mrm.26285.
58. Edzes, H.T., and Samulski, E.T. (1977). Cross relaxation and spin diffusion in the proton NMR or hydrated collagen. Nature *265*, 521-523. https://doi.org/10.1038/265521a0.
59. Gochberg, D.F., and Gore, J.C. (2003). Quantitative imaging of magnetization transfer using an inversion recovery sequence. Magnet Reson Med *49*, 501-505. https://doi.org/10.1002/mrm.10386.
60. Hamill, O.P., Marty, A., Neher, E., Sakmann, B., and Sigworth, F.J. (1981). Improved patch-clamp techniques for high-resolution current recording from cells and cell-free membrane patches. Pflügers Archiv *391*, 85-100. https://doi.org/10.1007/BF00656997.

1. Abdul Kadir, L., Stacey, M., and Barrett-Jolley, R. (2018). Emerging roles of the membrane potential: Action beyond the action potential. Frontiers in Physiology *9*, 1661. https://doi.org/10.3389/fphys.2018.01661.
2. Jefferys, J.G.R. (1995). Nonsynaptic modulation of neuronal activity in the brain: Electric currents and extracellular ions. Physiological Reviews *75*, 689-723. https://doi.org/10.1152/physrev.1995.75.4.689.
3. Helfant, R.H. (1986). Hypokalemia and arrhythmias. The American Journal of Medicine *80*, 13-22. https://doi.org/10.1016/0002-9343(86)90336-0.
4. Kane, C., Shepherd, R.M., Squires, P.E., Johnson, P.R.V., James, R.F.L., Milla, P.J., Aynsley-Green, A., Lindley, K.J., and Dunne, M.J. (1996). Loss of functional K_{ATP} channels in pancreatic

β-cells causes persistent hyperinsulinemic hypoglycemia of infancy. Nature Medicine *2*, 1344-1347. https://doi.org/10.1038/nm1296-1344.

5. Ling, G., and Gerard, R.W. (1949). The normal membrane potential of frog sartorius fibers. Journal of Cellular and Comparative Physiology *34*, 383-396. https://doi.org/10.1002/jcp.1030340304.
6. Neher, E., and Sakmann, B. (1976). Single-channel currents recorded from membrane of denervated frog muscle fibres. Nature *260*, 799-802. https://doi.org/10.1038/260799a0.
7. Tasaki, I., Watanabe, A., Sandlin, R., and Carnay, L. (1968). Changes in fluorescence, turbidity, and birefringence associated with nerve excitation. P Natl Acad Sci USA *61*, 883-888. https://doi.org/10.1073/pnas.61.3.883.
8. Tsien, R.Y. (1980). New calcium indicators and buffers with high selectivity against magnesium and protons: Design, synthesis, and properties of prototype structures. Biochemistry-Us *19*, 2396-2404. https://doi.org/10.1021/bi00552a018.
9. Zhou, Y., Liu, E., Müller, H., and Cui, B. (2021). Optical electrophysiology: Toward the goal of label-free voltage imaging. J Am Chem Soc *143*, 10482-10499. https://doi.org/10.1021/jacs.1c02960.
10. Berger, H. (1929). Über das elektrenkephalogramm des menschen. Archiv für Psychiatrie und Nervenkrankheiten *87*, 527-570. https://doi.org/10.1007/BF01797193.
11. Cohen, D. (1968). Magnetoencephalography: Evidence of magnetic fields produced by alpha-rhythm currents. Science *161*, 784-786. https://doi.org/10.1126/science.161.3843.784.
12. Mansfield, P. (1977). Multi-planar image formation using NMR spin echoes. Journal of Physics C: Solid State Physics *10*, L55-L58. https://doi.org/10.1088/0022-3719/10/3/004.
13. He, B., Sohrabpour, A., Brown, E., and Liu, Z. (2018). Electrophysiological source imaging: A noninvasive window to brain dynamics. Annu Rev Biomed Eng *20*, 171-196. https://doi.org/10.1146/annurev-bioeng-062117-120853.
14. Ogawa, S., Lee, T.-M., Nayak, A.S., and Glynn, P. (1990). Oxygenation-sensitive contrast in magnetic resonance image of rodent brain at high magnetic fields. Magnetic Resonanace in Medicine *14*, 68-78. https://doi.org/10.1002/mrm.1910140108.
15. Logothetis, N.K., Pauls, J., Augath, M., Trinath, T., and Oeltermann, A. (2001). Neurophysiological investigation of the basis of the fMRI signal. Nature *412*, 150-157. https://doi.org/10.1038/35084005.
16. Roth, B.J. (2023). Can MRI be used as a sensor to record neural activity? Sensors *23*, 1337. https://doi.org/10.3390/s23031337.
17. Bodurka, J., and Bandettini, P.A. (2002). Toward direct mapping of neuronal activity: MRI detection of ultraweak, transient magnetic fields changes. Magnet Reson Med *47*, 1052-1058. https://doi.org/10.1002/mrm.10159.
18. Konn, D., Gowland, P., and Bowtell, R. (2003). MRI detection of weak magnetic fields due to an extended current dipole in a conducting sphere: A model for direct detection of neuronal currents in the brain. Magnet Reson Med *50*, 40-49. https://doi.org/10.1002/mrm.10494.
19. Chow, L.S., Cook, G.G., Whitby, E., and Paley, M.N.J. (2006). Investigating direct detection of axon firing in the adult human optic nerve using MRI. NeuroImage *30*, 835-846. https://doi.org/10.1016/j.neuroimage.2005.10.024.
20. Xiong, J., Fox, P.T., and Gao, J.-H. (2003). Directly mapping magnetic field effects of neuronal activity by magnetic resonance imaging. Human Brain Mapping *20*, 41-49. https://doi.org/10.1002/hbm.10124.
21. Chu, R., de Zwart, J.A., van Gelderen, P., Fukunaga, M., Kellman, P., Holroyd, T., and Duyn, J.H. (2004). Hunting for neuronal currents: Absence of rapid MRI signal changes during visual-evoked response. NeuroImage *23*, 1059-1067. https://doi.org/10.1016/j.neuroimage.2004.07.003.
22. Luo, Q., Lu, H., Lu, H., Senseman, D., Worsley, K., Yang, Y., and Gao, J.-H. (2009). Physiologically evoked neuronal current MRI in a bloodless turtle brain: Detectable or not? NeuroImage *47*, 1268-1276. https://doi.org/10.1016/j.neuroimage.2009.06.017.

23. Parkes, L.M., de Lange, F.P., Fries, P., Toni, I., and Norris, D.G. (2007). Inability to directly detect magnetic field changes associated with neuronal activity. Magnet Reson Med *57*, 411-416. https://doi.org/10.1002/mrm.21129.
24. Toi, P.T., Jang, H.J., Min, K., Kim, S.-P., Lee, S.-K., Lee, J., Kwag, J., and Park, J.-Y. (2022). In vivo direct imaging of neuronal activity at high temporospatial resolution. Science *378*, 160-168. https://doi.org/10.1126/science.abh4340.
25. Lesage, F., and Lazdunski, M. (2000). Molecular and functional properties of two-pore-domain potassium channels. American Journal of Physiology: Renal Physiology *279*, F793-F801. https://doi.org/10.1152/ajprenal.2000.279.5.F793.
26. Ma, X.-Y., Yu, J.-M., Zhang, S.-Z., Liu, X.-Y., Wu, B.-H., Wei, X.-L., Yan, J.-Q., Sun, H.-L., Yan, H.-T., and Zheng, J.-Q. (2011). External Ba^{2+} block of the two-pore domain potassium channel TREK-1 defines conformational transition in its selectivity filter. Journal of Biological Chemistry *286*, 39813-39822. https://doi.org/10.1074/jbc.M111.264788.
27. Vaughan, P.F.T., Kaye, D.F., Ball, S.G., Reeve, H.L., and Peers, C. (1995). The effect of barium on [^{3}H]noradrenalin release from the human neuroblastoma SH-SY5Y. European Journal of Neuroscience *7*, 875-880. https://doi.org/10.1111/j.1460-9568.1995.tb01074.x.
28. Pottosin, I.I., Bonales-Alatorre, E., Valencia-Cruz, G., Mendoza-Magaña, M.L., and Dobrovinskaya, O.R. (2008). TRESK-like potassium channels in leukemic T cells. Pflügers Archiv *456*, 1037-1048. https://doi.org/10.1007/s00424-008-0481-x.
29. Bradbury, M.W.B., Segal, M.B., and Wilson, J. (1972). Transport of potassium at the blood-brain barrier. Journal of Physiology *221*, 617-632. https://doi.org/10.1113/jphysiol.1972.sp009771.
30. Filippidis, A.S., Zarogiannis, S.G., Ioannou, M., Gourgoulianis, K., Molyvdas, P.-A., and Hatzoglou, C. (2012). Permeability of the arachnoid and pia mater. The role of ion channels in the leptomeningeal physiology. Child's Nervous System *28*, 533-540. https://doi.org/10.1007/s00381-012-1688-x.
31. Walz, W. (2000). Role of astrocytes in the clearance of excess extracellular potassium. Neurochemistry International *36*, 291-300. https://doi.org/10.1016/S0197-0186(99)00137-0.
32. O'Donnell, M.E. (2009). Ion and Water Transport across the Blood-Brain Barrier. In Physiology and Pathology of Chloride Transporters and Channels in the Nervous System, F.J. Alvarez-Leefmans, and E. Delpire, eds. (Academic Press), pp. 585-606. https://doi.org/10.1016/B978-0-12-374373-2.00030-3.
33. Stanisz, G.J., Yoon, R.S., Joy, M.L.G., and Henkelman, R.M. (2002). Why does MTR change with neuronal depolarization? Magnet Reson Med *47*, 472-475. https://doi.org/10.1002/mrm.10071.
34. Autio, J.A., Shatillo, A., Giniatullin, R., and Gröhn, O.H. (2014). Parenchymal spin-lock fMRI signals associated with cortical spreading depression. Journal of Cerebral Blood Flow & Metabolism *34*, 768-775. https://doi.org/10.1038/jcbfm.2014.16.
35. Hazlewood, C.F., Chang, D.C., Nichols, B.L., and Woessner, D.E. (1974). Nuclear magnetic resonance transverse relaxation times of water protons in skeletal muscle. Biophysical Journal *14*, 583-606. https://doi.org/10.1016/S0006-3495(74)85937-0.
36. Didier, M.E.P., Tarun, O.B., Jourdain, P., Magistretti, P., and Roke, S. (2018). Membrane water for probing neuronal membrane potentials and ionic fluxes at the single cell level. Nature Communications *9*, 5287. https://doi.org/10.1038/s41467-018-07713-w.
37. Mathur-De Vré, R. (1980). The NMR Studies of water in biological systems. Progress in Biophysics and Molecular Biology *35*, 103-134. https://doi.org/10.1016/0079-6107(80)90004-8.
38. Lang, F., Busch, G.L., Ritter, M., Völkl, H., Waldegger, S., Gulbins, E., and Häussinger, D. (1998). Functional significance of cell volume regulatory mechanisms. Physiological Reviews *78*, 247-306. https://doi.org/10.1152/physrev.1998.78.1.247.
39. Fraser, J.A., and Huang, C.L.-H. (2004). A quantitative analysis of cell volume and resting potential determination and regulation in excitable cells. Journal of Physiology *559*, 459-478. https://doi.org/10.1113/jphysiol.2004.065706.

40. Hoffmann, E.K., Lambert, I.H., and Pedersen, S.F. (2009). Physiology of cell volume regulation in vertebrates. Physiological Reviews *89*, 193-277. https://doi.org/10.1152/physrev.00037.2007.
41. Le Bihan, D., Urayama, S.-i., Aso, T., Hanakawa, T., and Fukuyama, H. (2006). Direct and fast detection of neuronal activation in the human brain with diffusion MRI. P Natl Acad Sci USA *103*, 8263-8268. https://doi.org/10.1073/pnas.0600644103.
42. Le Bihan, D. (2012). Diffusion, confusion and functional MRI. NeuroImage *62*, 1131-1136. https://doi.org/10.1016/j.neuroimage.2011.09.058.
43. Mangia, S., Chamberlain, R., De Martino, F., Moeller, S., Corum, C., Kim, T., Kalavagunta, C., Michaeli, S., Garwood, M., Kim, S.-G., and Ugurbil, K. (2012). Functional MRI with SWIFT. Proceedings of International Society of Magnetic Resonance in Medicine *20*, 0326.
44. Ferreira, G., Yi, J., Ríos, E., and Shirokov, R. (1997). Ion-dependent inactivation of barium current through L-type calcium channels Journal of General Physiology *109*, 449-461. https://doi.org/10.1085/jgp.109.4.449.
45. Findlay, I. (2002). Voltage- and cation-dependent inactivation of L-type Ca^{2+} channel currents in guinea-pig ventricular myocytes. Journal of Physiology *541*, 731-740. https://doi.org/10.1113/jphysiol.2002.019729.
46. Zhang, B.-X., Zhao, H., Loessberg, P.A., and Muallem, S. (1992). Regulation of agonist-evoked $[Ca^{2+}]_i$ oscillation by intracellular Ca^{2+} and Ba^{2+} in AR42J cells. American Journal of Physiology: Cell Physiology *262*, C1125-C1133. https://doi.org/10.1152/ajpcell.1992.262.5.C1125.
47. Liu, Y.-J., Grapengiesser, E., Gylfe, E., and Hellman, B. (1994). Glucose-induced oscillations of Ba^{2+} in pancreatic β-cells occur without involvement of intracellular mobilization. Archives of Biochemistry and Biophysics *315*, 387-392. https://doi.org/10.1006/abbi.1994.1515.
48. Thomas, R.C. (2009). The plasma membrane calcium ATPase (PMCA) of neurones is electroneutral and exchanges 2 H^+ for each Ca^{2+} or B^{a2}+ ion extruded. Journal of Physiology *587*, 315-327. https://doi.org/10.1113/jphysiol.2008.162453.
49. Lee, S.-H., Han, M.-J., Lee, J., and Lee, S.-K. (2020). Experimental setup for bulk susceptibility effect-minimized, multi-orientation MRI of *ex vivo* tissue samples. Medical Physics *47*, 3032-3043. https://doi.org/10.1002/mp.14174.
50. Li, K., Zu, Z., Xu, J., Janve, V.A., Gore, J.C., Does, M.D., and Gochberg, D.F. (2010). Optimized inversion recovery sequences for quantitative T_1 and magnetization transfer imaging. Magnetic Resonanace in Medicine *64*, 491-500. https://doi.org/10.1002/mrm.22440.
51. Dreier, J.P., Körner, K., Görner, A., Lindauer, U., Weih, M., Villringer, A., and Dirnagl, U. (1995). Nitric oxide modulates the CBF response to increased extracellular potassium. J Cerebr Blood F Met *15*, 914-919. https://doi.org/10.1038/jcbfm.1995.116.
52. Redmond, L., Kashani, A.H., and Ghosh, A. (2002). Calcium regulation of dendritic growth via CaM kinase IV and CREB-mediated transcription. Neuron *34*, 999-1010. https://doi.org/10.1016/s0896-6273(02)00737-7.
53. Mostany, R., and Portera-Cailliau, C. (2008). A craniotomy surgery procedure for chronic brain imaging. Journal of Visualized Experiments, e680. https://doi.org/10.3791/680.
54. McPhee, K.C., and Wilman, A.H. (2017). Transverse relaxation and flip angle mapping: Evaluation of simultaneous and independent methods using multiple spin echoes. Magnet Reson Med *77*, 2057-2065. https://doi.org/10.1002/mrm.26285.
55. Edzes, H.T., and Samulski, E.T. (1977). Cross relaxation and spin diffusion in the proton NMR or hydrated collagen. Nature *265*, 521-523. https://doi.org/10.1038/265521a0.
56. Gochberg, D.F., and Gore, J.C. (2003). Quantitative imaging of magnetization transfer using an inversion recovery sequence. Magnet Reson Med *49*, 501-505. https://doi.org/10.1002/mrm.10386.
57. Hamill, O.P., Marty, A., Neher, E., Sakmann, B., and Sigworth, F.J. (1981). Improved patch-clamp techniques for high-resolution current recording from cells and cell-free membrane patches. Pflügers Archiv *391*, 85-100. https://doi.org/10.1007/BF00656997.